Nanoscale mapping of potential barrier degradation at BaTiO3-Ni interfaces

Journal:	*ACS Applied Electronic Materials*
Manuscript ID	el-2021-00852f.R1
Manuscript Type:	Article
Date Submitted by the Author:	n/a
Complete List of Authors:	Morelli, Alessio; University of Ulster School of Engineering, NIBEC Mc Laughlin, Garry ; University of Ulster School of Engineering, NIBEC Strawhorne , Maureen ; AVX Ltd Byrne, John; NIBEC, Engineering Lemoine, Patrick; University of Ulster at Jordanstown, NIBEC

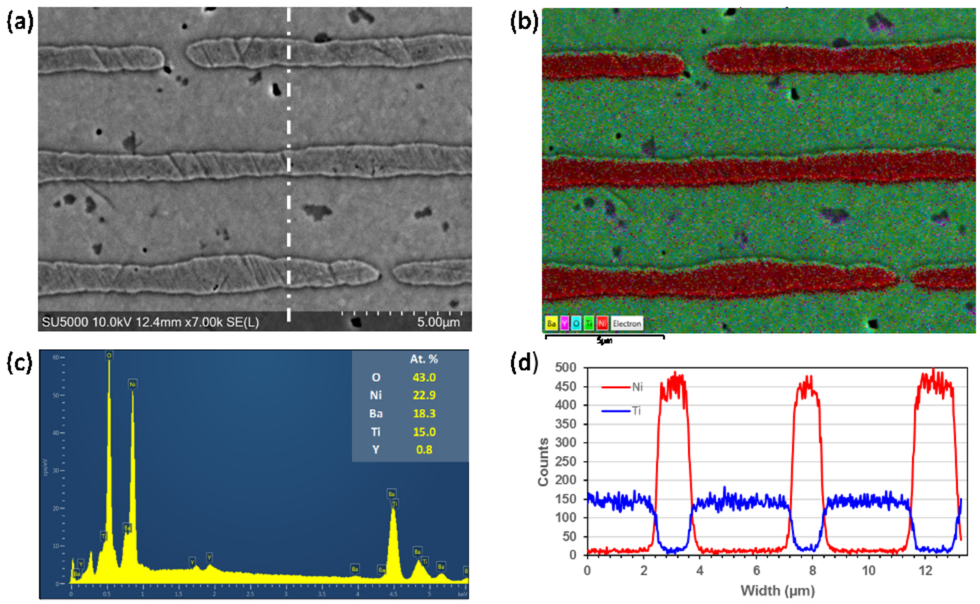

Figure 1: (a) SEM high vacuum secondary electron detector image of a fresh capacitor, (b) and with overlapped Energy Dispersive X-Ray Spectroscopy (EDS) signal, (c) EDS spectrum and (d) line profiles of the EDS signal obtained from line marked in (a).

84x52mm (300 x 300 DPI)

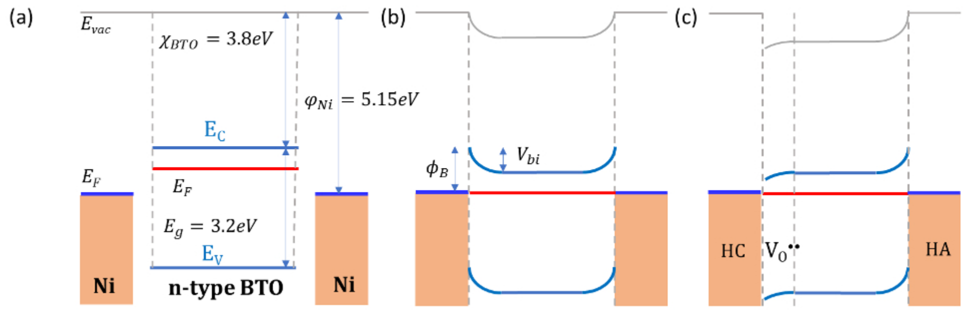

Figure 2: Band diagrams for metal-semiconductor-metal configuration with Ni electrodes and n-type BTO for a zero bias: (a) flat band diagram for fresh capacitor, diagram after contact for (b) fresh and (c) aged capacitor with oxygen vacancies accumulation at the HALT cathode (HC). HALT anode is labelled as HA.

84x26mm (300 x 300 DPI)

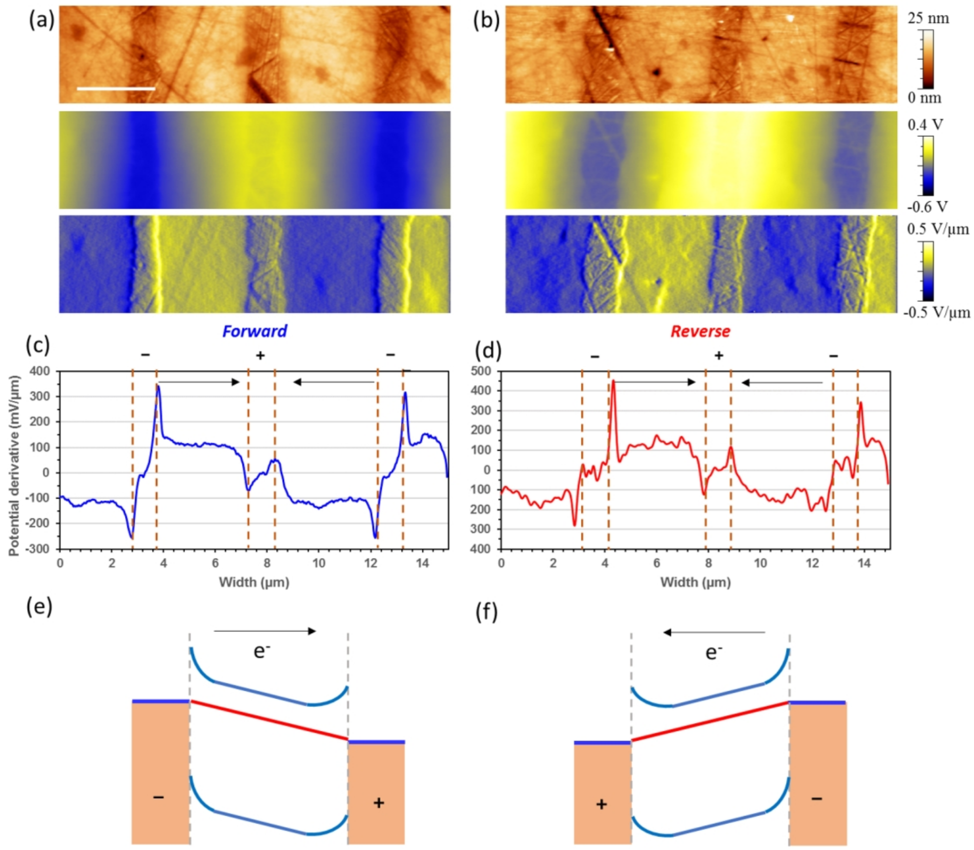

Figure 3: Kelvin probe microscopy of fresh capacitor under external bias of 1V: (a,b) topography, KPFM potential, derivative of potential, (c,d) Y average of potential derivative, (e,f) band diagram for forward and reverse bias respectively. The discontinuities at dielectric-electrode interface are a signature of Schottky contacts. As expected for n-type semiconductor and fresh MLCCs, higher discontinuities appear at negatively biased electrodes, regardless of biasing configuration. Vertical broken lines in plots c-d identify electrodes' positions; labels over plots c-d indicate the polarity of external applied bias. Scalebar in (a) is 3µm.

141x121mm (300 x 300 DPI)

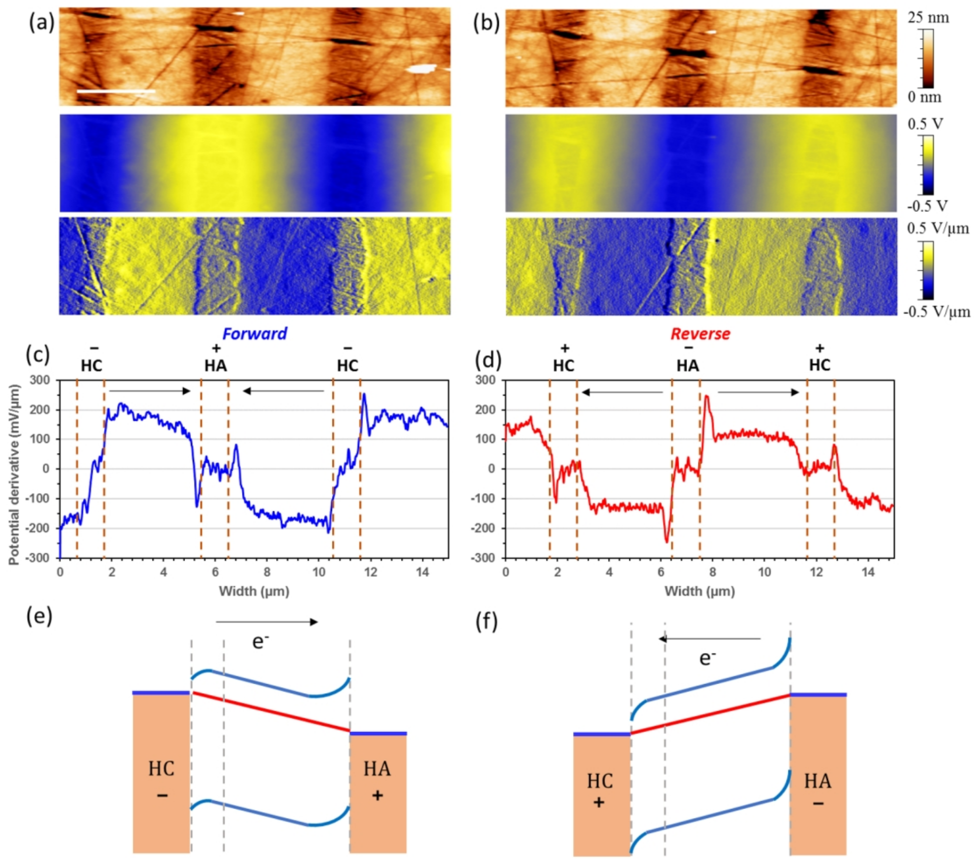

Figure 4: Kelvin probe microscopy of aged capacitor (150 min HALT) under external bias of 1V: (a,b) topography, KPFM potential, derivative of potential, (c,d) Y average of potential derivative , (e,f) band diagram for forward and reverse bias respectively. The discontinuities display higher value at the interfaces with the HALT anode, regardless of bias configuration. Vertical broken lines in plots c-d identify electrodes' positions; labels over plots c-d indicate the polarity of external applied bias and cathode (HC) and anode (HA) during HALT procedure. Scalebar in (a) is 3µm.

141x121mm (300 x 300 DPI)

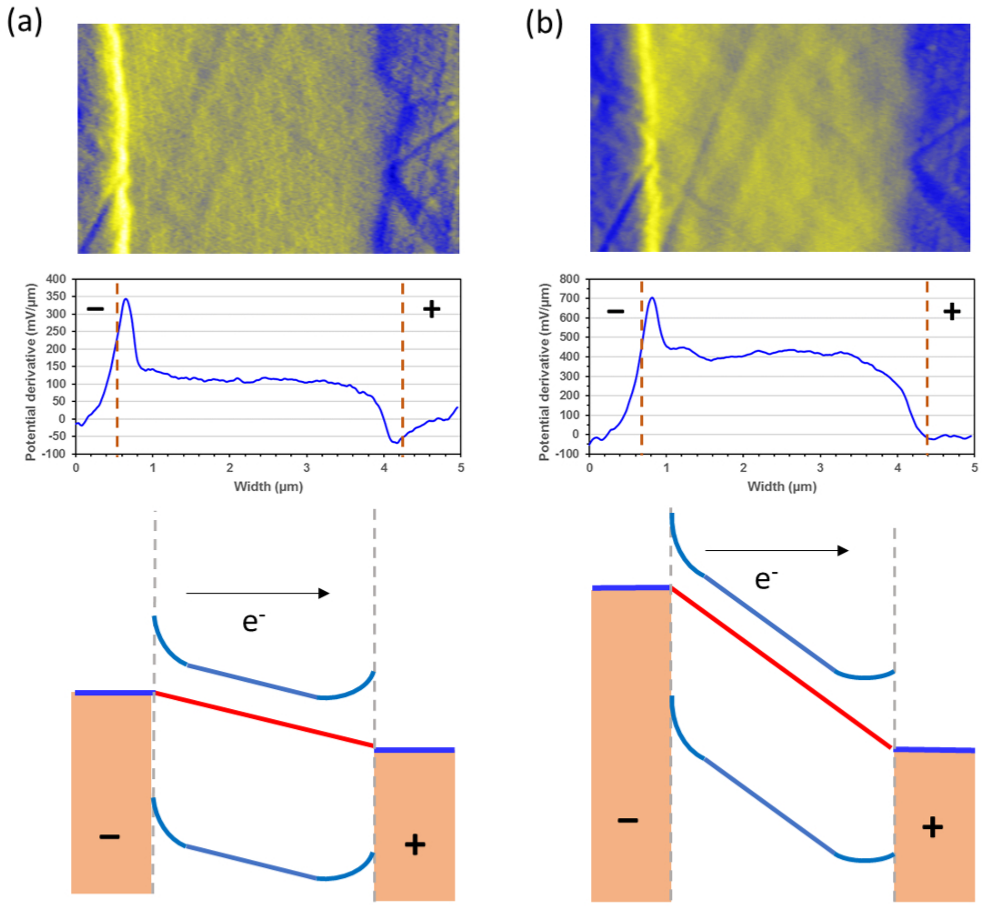

Figure 5: Kelvin probe microscopy of capacitors under increasing external bias: potential derivative, Y average plot of the same and band diagram of fresh capacitor at (a) 1V and (b) 3V. The disappearance of discontinuity at the positive electrode at 3V matches decrease of built-in bias with increasing applied voltage. Note: (a) is an extract of the data shown in figure 3a.

84x78mm (300 x 300 DPI)

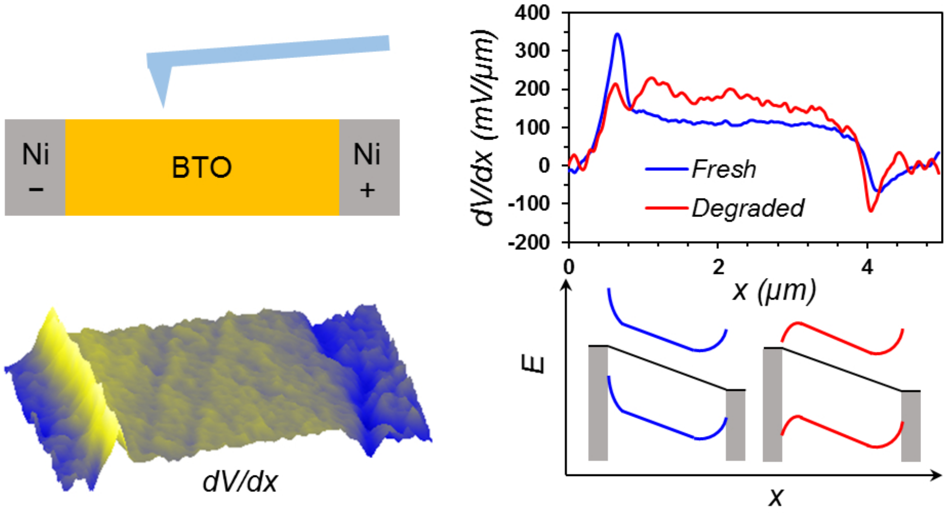

82x44mm (300 x 300 DPI)

Nanoscale mapping of potential barrier degradation at $BaTiO_3$-Ni interfaces

Alessio Morelli[a,*], *Garry McLaughlin*[a], *Maureen Strawhorne*[b], *John Anthony Byrne*[a], *Patrick Lemoine*[a]

[a] NIBEC, Ulster University, Shore Road, Newtownabbey BT37 0QB, United Kingdom

[b] AVX Ltd, 5 Hillman's Way, Coleraine BT52 2DA, United Kingdom

ABSTRACT

Scanning Kelvin probe microscopy was used to investigate the evolution of the Ni-BaTiO3 interfacial potential barriers in multilayer ceramic capacitors degraded by High Accelerated Life Testing. We detect electric field discontinuities at such interfaces which, by analyzing the expected band diagrams, are associated to the presence of Schottky barriers. The decrease of discontinuities at the cathode in degraded capacitors denotes barrier lowering, indicative of a transition from Schottky to Ohmic contact, validating the proposed mechanism of oxygen vacancies electromigration being at the origin of insulation resistance degradation.

Extrapolation of depletion layer width is consistent with previous observations, and the possibility towards the use of this technique to obtain quantitative information is discussed.

KEYWORDS

Barium titanate, Nickel, Schottky barrier, Kelvin Probe Microscopy, Multilayer Ceramic Capacitor, Degradation

INTRODUCTION

Among the many applications based on ferroelectric oxides, Multilayer Ceramic Capacitors (MLCCs) are used in most electronic devices [1–3]. Being constructed of interdigitated metal electrodes in a matrix of dielectric material, most commonly conductive Nickel and high-k ceramic barium titanate (BTO) are employed [3]. Since the progress in MLCCs saw the switch to base metal electrodes and with their progressive miniaturization, leakage mechanism (so-called insulation resistance degradation) has become more critical as a cause of failure [4]. The cost-driven move from palladium to nickel electrodes posed the issue of avoiding electrode oxidation during co-firing, leading to the solution of performing such step in low oxygen pressure atmosphere [2]. However, the remedy led to the drawback of oxygen vacancies formation in the dielectric layers, which, despite the addition of a further re-oxidizing step in the manufacturing process [5,6], gives raise to leakage issues.

It is already well established that aging and fatigue in ferroelectrics are caused by defects in the oxide material, with interface effects playing a major role, whereby charged defects diffuse to grain boundaries and interfaces [7]. Similarly, in MLCCs the oxygen vacancies in the dielectric BTO layers under DC electric field accumulate at grain boundaries and metal-oxide interfaces [5,8], causing eventually component failure by insulation resistance degradation.

In fact, electrical characterization investigations [8,9] have highlighted that the main contribution to the total resistance comes from interfacial contact resistance at the electrode-dielectric interface. Impedance spectroscopy on progressively degraded samples showed a drastic decrease in resistance at the metal-dielectric interface, with less pronounced decrease at the grain boundaries and negligible within the grains. Based on these results, it was deduced that Schottky barriers at the metal-oxide interface lower with degradation of the device, finally turning into Ohmic contacts, with free flow of carriers through conductive paths [10] ultimately leading to failure due to Joule heating. The process, as revealed by Transmission Electron Microscopy [9], is linked to oxygen vacancies first accumulating at the grain boundaries and finally migrating towards the cathode electrode, where they result in progressive lowering of Schottky barrier.

Although the migration of oxygen vacancies has been verified and the mechanism leading to failure has been documented by macroscopic measurements, the actual barrier lowering from degradation is still to be demonstrated at the nanoscale. A recent X-ray Photoelectron Spectroscopy (XPS) study confirmed the presence and quantified the height [11] of potential barriers at Ni-BTO interfaces, although without lateral resolution. A good candidate technique to perform such nanoscale measurements is Kelvin Probe Force Microscopy (KPFM) which can give high spatial resolution surface potential measurements [12], providing information about a device band structure [13–16]. However, KPFM investigations of MLCC degradation are scarce [17–19] and give mitigated results; they point to an increase of barrier height at the interfaces with degradation, which would be consistent with a p-type semiconducting BTO. Still, co-firing in reducing atmosphere leads to presence of oxygen vacancies, and the consensus in the published literature [5,8,11,20,21] is that in such case BTO is a n-type semiconductor. There are indeed reports of p-type semiconducting BTO at high temperatures [21], high oxygen pressure [22], and with Yttrium doping over 2mol% [23], conditions not matched during operation or processing of MLCCs. Hence until now the mechanism underlying insulation resistance degradation has not been validated by nanoscale investigations.

Here we explore the evolution of Schottky barriers at the metal-semiconductor Ni-BTO interface by carrying out KPFM measurements on polished MLCCs under external applied bias, progressively degraded by Highly Accelerated Life Test (HALT) [24,25]. We link discontinuities in the gradient of contact potential difference measured by KPFM to the presence of interface barriers by use of predicted band diagrams, in order to elucidate barriers degradation. Ultimately, we provide proof that MLCC degradation progresses with a lowering of the potential barrier height at the cathode. This has not been previously demonstrated at the nanoscale using KPFM measurements and the revealed trend is consistent with macroscopic electrical measurements and at the origin of MLCCs failure by insulation resistance degradation.

MATERIALS AND METHODS

X7R-type 1206 parts (AVX Ltd, Coleraine) with a dielectric layer of 3.8 μm and a capacitance of 10 μF were used for the investigations. They were manufactured using a BTO-based dielectric and Ni base metal electrodes (BME), in a multilayer design to produce MLCCs. In order to enhance reliability, acceptors were added at concentrations of less than 1 mol%. The parts were sintered in a reducing atmosphere, at temperatures ranging from 1100 to 1350˚C and in oxygen pressure in the range 10^{-6} – 10^{-12}Pa depending upon the Ni/NiO equilibrium at the sintering temperature to avoid BME oxidation. Despite the addition of acceptor dopants in the dielectric, a small concentration of oxygen vacancies remains in the sintered structure, which was lowered by annealing in a weakly oxidizing atmosphere (800 – 1100˚C, pO_2 10^{-1}– 10^{-8}Pa), with oxygen pressure high enough to reduce the oxygen vacancy concentration, and yet low enough to inhibit NiO formation. The used R&D parts were prepared with the same industrial manufacturing system and methodology as for AVX automotive grade parts, hence site the tolerances in capacitance, geometrical dimensions, etc. for these automotive parts (i.e., a public domain information) as indicative of the tolerances for the R&D parts here studied.

Selected capacitors were degraded by HALT at 100V and 150°C for 150 minutes, to be compared with fresh samples. The median time to fail under the above-mentioned conditions was estimated to be about 180 minutes.

Fresh and degraded samples were positioned on a sample mount with arranged silver paste connections to the MLCCs contact electrodes, and mirror polished by chemical mechanical polishing (CMP - Struers TegraPol 31) to expose the interdigitated inner Ni electrodes.

Kelvin probe force microscopy was performed in air with a D3100 atomic force microscope (AFM) from Bruker ltd., using platinum coated silicon probes (FMV-PT Bruker, nominal spring constant 2.8 Nm^{-1}, resonance frequency 75 kHz, radius of curvature 25 nm), following the standard two-pass procedure [12]. A first pass in amplitude modulation AFM with cantilever mechanically oscillating close to resonance records the topography; during a second pass AC voltage ($3V_{rms}$ at resonance) is applied to the probe (not mechanically excited) kept at a constant distance from the surface (lift height 10 nm) by using the information obtained during the first pass; the electrostatic interaction resulting from AC voltage on the probe and probe-sample contact potential difference induces the probe to vibrate; in order to nullify the vibration a feedback loop applies to the probe a DC voltage corresponding to the local probe-sample contact potential difference, the value of which is mapped. The measurements were performed under external bias varying from 1 to 3V (2.6 to 7.9 kV/cm, considering the average dielectric thickness of 3.85 μm) applied across the MLCCs interdigitated electrodes by wiring the prepared contacts on the sample mount to a DC power supply (Thandar TS3021S). Voltage applied in the same direction as employed for HALT procedure (positive voltage to the HALT anode and negative voltage to HALT cathode) will be referred hereafter as forward bias, while the opposite configuration will be termed reverse bias.

The potential provided by KPFM corresponds to the contact potential difference, which relates to the work function of the probe (ϕ_{Probe}) and of the sample (ϕ_{Sample}) as

$$V_{CPD} = \frac{\phi_{Probe} - \phi_{Sample}}{e} \#$$

and therefore, assuming ϕ_{Probe} to be constant throughout the measurement, changes in V_{CPD} are proportional to changes in ϕ_{Sample}. Being the work function the difference between vacuum level and Fermi level, a band bending at the interface - yielding a synchronal bending of the vacuum level - results in a change of sample's work function. Hence, monitoring variations in KPFM potential under external applied bias yields local information about changes in the band structure in the system under study [14,16].

High vacuum scanning electron microscopy (SEM – SU5000 FEGSEM Hitachi Ltd) was employed to characterize the morphology (secondary electron detector imaging, 10kV acceleration voltage) and chemical composition (Energy Dispersive X-Ray Spectroscopy – EDS - Oxford Instrument Aztec system) of the mirror polished samples.

Image analysis and elaboration has been performed via the program WSxM [26].

RESULTS AND DISCUSSION

Morphology and compositional details of the polished MLCCs obtained by SEM (Figure 1) confirm BTO dielectric layers and Ni electrodes with thicknesses of about 3.8μm and 1.2μm respectively. Traces of Yttrium (<1%) are detected within the BTO layer (1b-c), a trivalent amphoteric dopant widely used to improve MLCCs reliability [23,27,28].

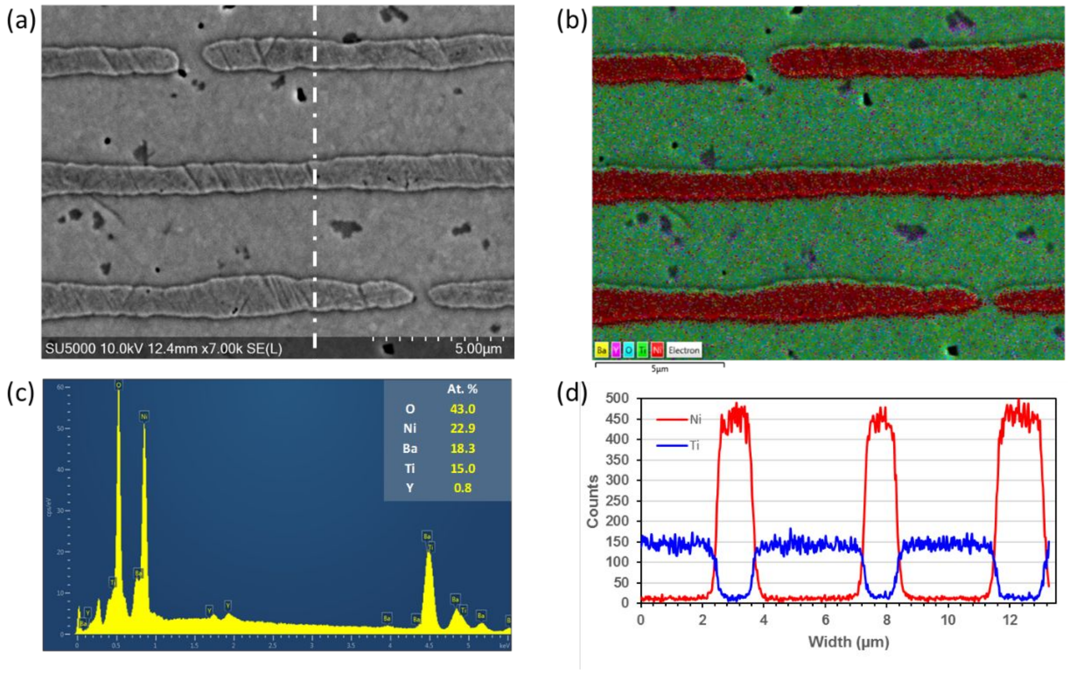

Figure 1: (a) SEM high vacuum secondary electron detector image of a fresh capacitor, (b) and with overlapped Energy Dispersive X-Ray Spectroscopy (EDS) signal, (c) EDS spectrum and (d) line profiles of the EDS signal obtained from line marked in (a).

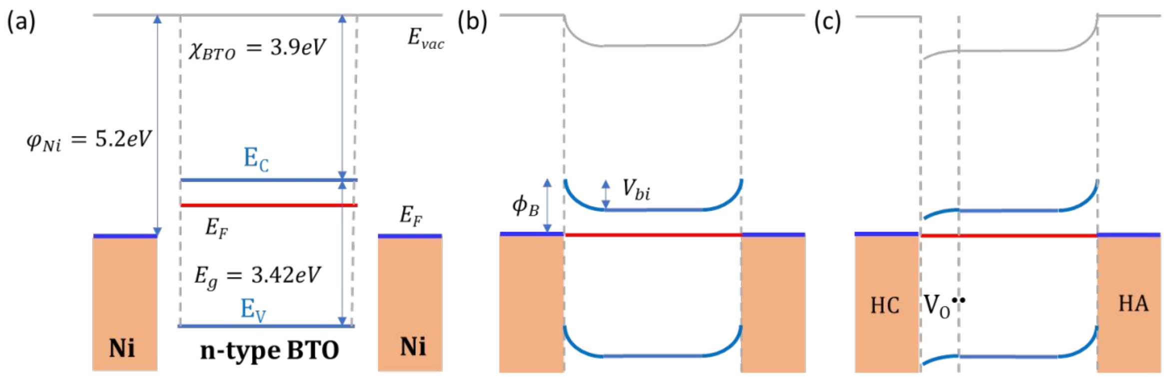

Figure 2: Band diagrams for metal-semiconductor-metal configuration with Ni electrodes and n-type BTO for a zero bias: (a) flat band diagram for fresh capacitor, diagram after contact for

(b) fresh and (c) degraded capacitor with oxygen vacancies accumulation at the HALT cathode (HC). HALT anode is labelled as HA.

In order to correctly interpret the results, it is useful to anticipate the expected behavior of the Ni-BTO-Ni capacitor based on the corresponding band diagrams (Figure 2). In first place, having BTO been exposed to a reducing atmosphere at high temperature during the production process, it is an n-type semiconductor [11,20,21,29] (figure 2a). Therefore, the phenomenology for metal-semiconductor junctions can be applied in this case, and, considering only the interfaces, the Ni-BTO-Ni system can be treated as two back-to-back Schottky diodes [30]. The contribution of grain boundaries is indeed relevant, with double Schottky barriers to be considered in the diagram (figure S1). However, being the analysis of the barriers at the grain boundaries out of the scope of this manuscript, and for sake of clarity of representation, we opted for a simplified version of the band diagram.

With a BTO electron affinity (χ_{BTO} = 3.9 eV) [31] higher than the Ni work function (φ_{Ni} = 5.1 eV) [32] and the Fermi level energy of BTO close to the conduction band edge (E_C-E_F^{BTO}=0.34eV) [11], in the case of a fresh capacitor, an upward band bending occurs at both interfaces; the two Schottky junctions are identical, displaying the same value of barrier height ϕ_B and built-in potential V_{bi} (figure 2b). For a degraded capacitor the accumulation of oxygen vacancies at the HALT cathode causes electrons to migrate from the electrode into the BTO to compensate the positive charge accumulation [33], locally raising the Fermi level value, hence at equilibrium bending the bands downwards (figure 2c) at that interface and lowering the Schottky barrier height [34,35]. As the junction at the HALT anode interface is unchanged, the expected band diagram of the degraded capacitor should display an asymmetric configuration.

With the configuration of figure 2b, the potential barriers limit charge carriers' migration from the electrodes into the dielectric and vice-versa providing the system with high resistivity, while the barrier lowering as in figure 2c results in an increase in leakage current (or insulation resistance degradation) eventually leading to device's failure.

For the Ni-BTO-Ni system under external bias V_a (Figure 3e-f and 4e-f) the Fermi levels of the two electrodes are shifted with respect to each other by the value eV_a, and the Fermi level of BTO is not a constant anymore, but slopes between the two metal's levels. Additionally, corrections for the potential barriers' height should be taken in account [36,37], but while the change in built-in potential V_{bi} (diminished by the value of applied bias) is significant, for Schottky barrier height it is negligible due to the high relative permittivity of BTO and low applied fields.

Most notably, the resulting metal-semiconductor-metal band diagrams for fresh capacitors under external bias exhibit configurations for forward (Figure 3e) and reverse (Figure 3f) bias mirroring each other, a trait not featured by the band diagrams for degraded capacitors (Figure 4e and 4f) due to the lower barrier at the HALT cathode interface.

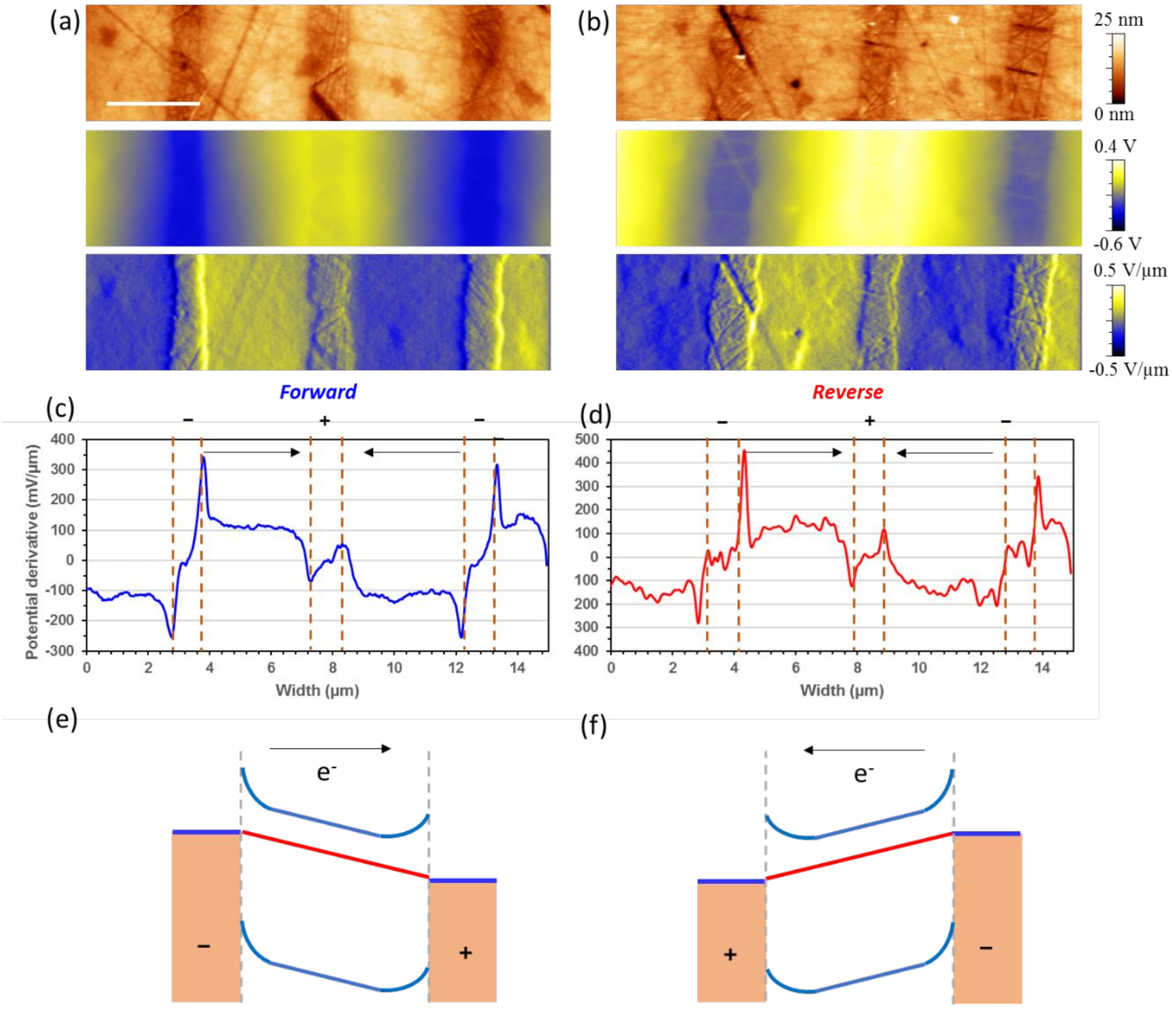

Figure 3: Kelvin probe microscopy of fresh capacitor under external bias of 1V: (a,b) topography, KPFM potential, derivative of potential, (c,d) Y average of potential derivative, (e,f) band diagram for forward and reverse bias respectively. The discontinuities at dielectric-electrode interface are a signature of Schottky contacts. As expected for n-type semiconductor

and fresh MLCCs, higher discontinuities appear at negatively biased electrodes, regardless of biasing configuration. Vertical broken lines in plots c-d identify electrodes' positions; labels over plots c-d indicate the polarity of external applied bias. Scalebar in (a) is 3μm.

A first set of KPFM measurements was conducted with external voltage of 1V in forward and reverse bias (Figure 3) on a fresh sample, providing simultaneously images of the topography and the KPFM potential. The topography (top images in Fig.3a and 3b) shows nickel electrodes at a slightly lower height (~10 nm) than BTO, because of its lower hardness and, consequently, higher removal rate during the polishing process, with a roughness $R_a = 2.7$ nm. The width values of the alternated layers in this AFM image are in agreement with the ones obtained by SEM measurements. KPFM potential (middle images in Fig.3a and 3b) slopes from the positive to the negative electrode confirming that the external bias is applied to the dielectric layers. Changes in potential reflect changes in work-function – and hence carriers band energy - across the sample. Being the work function the difference between vacuum level energy and Fermi level energy, band bending at the interface yields a change in work function. Hence, superimposed to the sloping potential given by the bias applied across the dielectric layer, finer changes are to be expected in correspondence of Schottky barriers. A derivative of the KPFM potential (bottom images in Fig.3a and 3b) clearly reveals large discontinuities at the Ni-BTO interfaces and a less pronounced modulation within the dielectric layers. Y-averages of the potential derivative images (Fig.3c and 3d) evidence the discontinuities at the interface, clearly displaying different magnitudes at the interfaces depending on the electrode's poling. The magnitude of the discontinuities at the interface with positively poled electrodes is usually bigger than the corresponding one at the negatively poled electrode (Figure 3c), and this behavior holds as well upon bias reversal (Figure 3d). Relating the KPFM measurement with the expected band diagrams (Figure 3e and f), it can be observed that the electrons in the conduction band have energies with a higher gradient at the negatively poled electrode than the ones at the positively poled one, due to the correction of V_{bi} under external applied bias. Hence the expected potential derivative from KPFM is expected to be higher in magnitude at the negatively poled electrode, in agreement with what is seen in Fig.3c and 3d, no matter if the experiment is performed in forward or reverse bias. This proves that the charge carriers are electrons, hence confirming that due to the processing conditions of MLCCs, the BTO is indeed n-type, as is the consensus [5,8,11,20,21] and in contradiction to earlier KPFM studies [17,18].

Before progressing with the discussion, it is worthwhile to observe that in the potential derivative images (bottom of fig.3a and 3b) the presence of crosstalk from the topography can be discerned until a certain extent, with the marks from CMP polishing clearly noticeable.

However, the fact that the magnitude of the potential derivative discontinuities at the interfaces modulates with the poling sign of the electrodes (fig.3c and 3d) indicates that these features are not to be ascribed to topographic crosstalk. In support of this, apart from the overlapping of KPFM potential signal in trace and retrace (not shown here), additional experiments will be discussed subsequently in this work. Furthermore, the presence of a less pronounced pattern of modulated potential derivative can be observed in the dielectric layers in figures 3a and 3b, which is usually indicative of double Schottky barriers expected at grain boundaries in ceramic oxides [5,38]. However, in this case the influence of topographic crosstalk on these features cannot be completely excluded, hence, being as well their analysis beyond the scope of this article, they will not be treated in the present work.

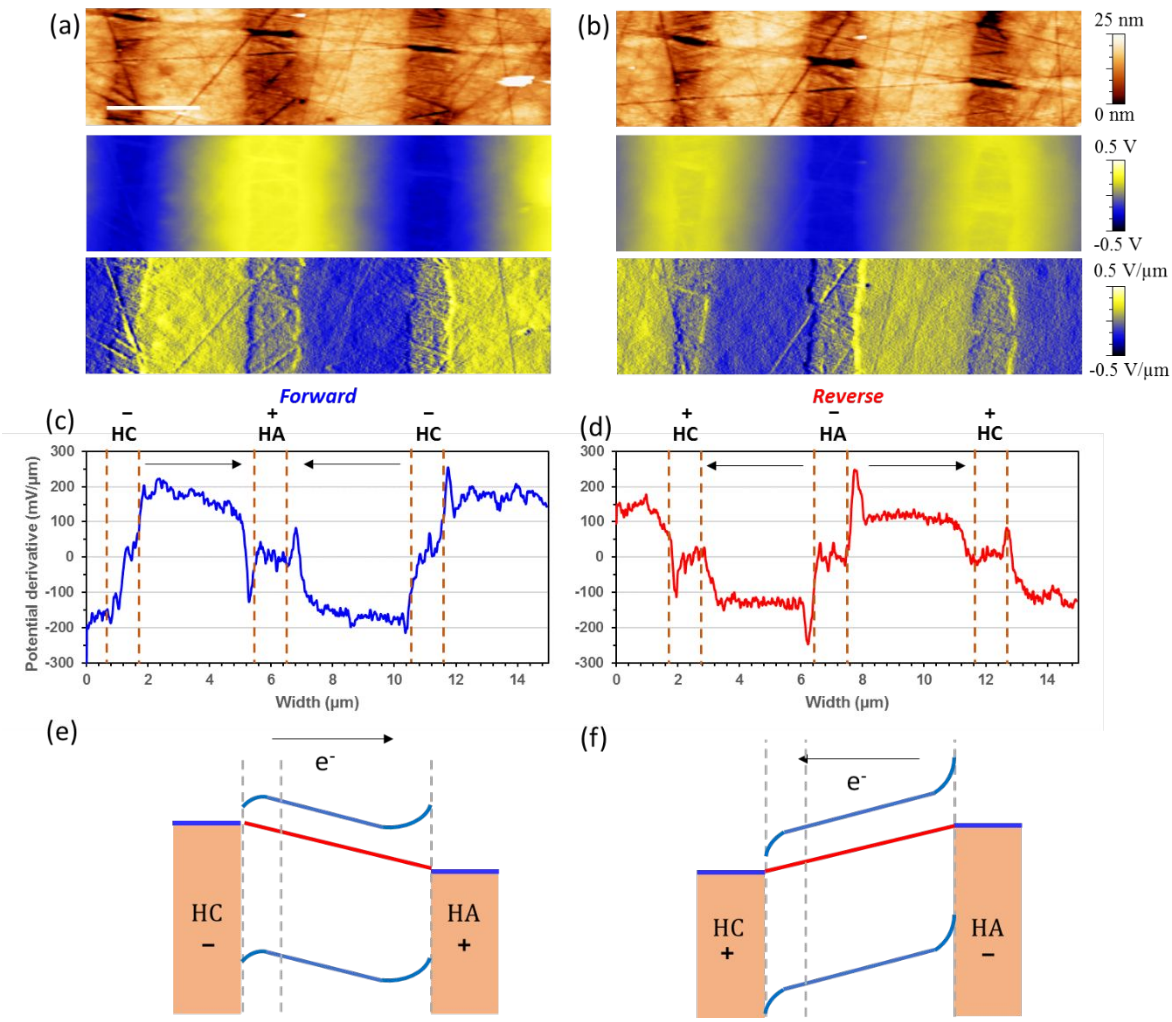

Figure 4: Kelvin probe microscopy of degraded capacitor (150 min HALT) under external bias of 1V: (a,b) topography, KPFM potential, derivative of potential, (c,d) Y average of potential derivative , (e,f) band diagram for forward and reverse bias respectively. The discontinuities display higher value at the interfaces with the HALT anode, regardless of bias configuration. Vertical broken lines in plots c-d identify electrodes' positions; labels over plots c-d indicate the polarity of external applied bias and cathode (HC) and anode (HA) during HALT procedure. Scalebar in (a) is 3µm.

Results from KPFM measurements on a degraded capacitor (Figure 4) display substantially different potential maps. The potential derivative (bottom of figure 4a and 4b) reveals the presence of barriers at the interfaces, but the Y-average of such images (figure 4c and 4d) evidences a different behavior, with KPFM potential derivative showing significant discontinuities at the HALT anode both for forward and reverse bias, while discontinuities at the HALT cathode interface being mostly very small in magnitude. Furthermore, it can be observed that the discontinuities at a given interface are lower for the positively biased electrode. Interpretation of the KPFM results by means of the expected band diagrams (figure 4e and f) evidences a match between them, with the discontinuities at the HALT anode interface corresponding to the fully preserved Schottky barrier in the band diagram, and the smaller discontinuities at the HALT cathode interface corresponding to the barrier lowering (and consequently lower gradient of conduction band energy) due to downward band bending caused by oxygen vacancy accumulation.

The experimental data in figures 3 and 4, with the aid of band diagram interpretation, provide experimental proof at the nanoscale of the electrical behavior at the interfaces in fresh and degraded capacitors, namely a trend in which the Schottky barrier height at the capacitor's cathode lowers with capacitor degradation. This matches the interpretation given based on macroscopic electrical measurements and TEM analysis [5,8,9]: with degrading of the capacitor, the accumulation of oxygen vacancies at the HALT cathode yields lowering of Schottky barrier height, until there is a transition from Schottky to Ohmic contact, responsible for insulation resistance degradation.

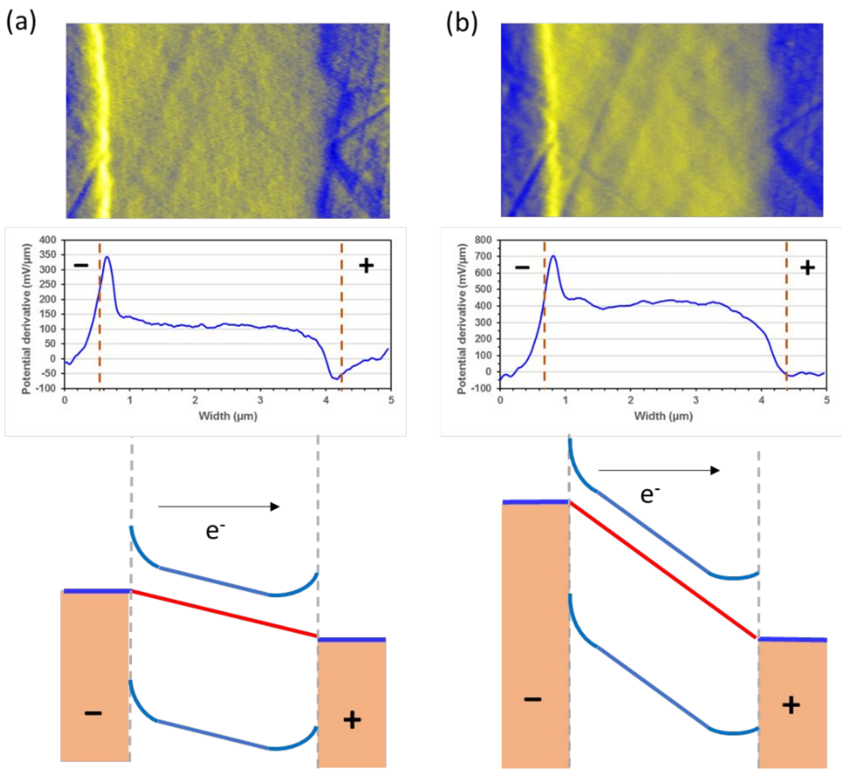

Figure 5: Kelvin probe microscopy of capacitors under increasing external bias: potential derivative, Y average plot of the same and band diagram of fresh capacitor at (a) 1V and (b) 3V. The disappearance of discontinuity at the positive electrode at 3V matches decrease of built-in bias with increasing applied voltage. Note: (a) is an extract of the data shown in figure 3a.

To further verify the origin of discontinuities of potential derivative at the interfaces, namely, to indisputably relate them with presence of Schottky barriers, and to exclude their link with topographic crosstalk, we performed further experiments with increasing applied external bias [13]. KPFM potential was acquired over a fresh capacitor under forward bias of 1V (figure 5a) and 3V (figure 5b) consecutively. Potential derivative maps (top of figure 5) evidence discontinuities at the interfaces. Y-average plots (middle of figure 5) clearly evidence that the discontinuity at the positively biased electrode does not change its magnitude with increasing of external bias, while the discontinuity at the negatively biased electrode disappears. Interpretation of the results considering the corresponding band diagrams (bottom of figure 5) clearly relates the disappearance of the discontinuity at the positive electrode with the band flattening due to the increase of external applied bias. A complete set of experiments have been performed with the same procedure in reverse bias and forward bias for fresh and degraded capacitors, yielding the same results (figures S4 and S5). Therefore, we can confirm that the discontinuities in potential derivative at the electrode interfaces are related to the presence of potential barriers and do not originate from topographic crosstalk.

Finally, we would like to point out the wealth of information that potentially KPFM investigations can provide on potential barriers and electronic properties. For instance, the discontinuity width can be related to the depletion layer thickness, from which density of accumulated impurities [37,38] can be calculated, and eventually information about barrier height could be obtained [14]. From figure 3 and 4 the FWHM of the discontinuities related to the negatively poled electrodes has been measured, yielding an average of 200nm for the as-produced and 73nm for degraded interfaces. These values are comparable with data from literature obtained by KPFM in UHV [17] and with the width of oxygen vacancy accumulation region measured by TEM [5,9]. Under the abrupt approximation of donor concentration $N_D \neq 0$ only within the depletion layer, from the formulas for depletion thickness W_D and maximum electric field E_{max}, the donor concentration can be calculated as

$$N_D = \frac{\epsilon_0 \epsilon_r E_{max}}{e W_D}$$

with e the electron charge, ϵ_0 the dielectric permittivity of vacuum and ϵ_r the relative permittivity of BTO. By using a conservative value of 2000 for the relative permittivity of BTO [3] and measuring the values for W_D and E_{max} from the second discontinuity in figure 3c (barrier at electrode in fresh capacitor) and the one at the second cathode interface in figure 4c (barrier at cathode in degraded capacitor), a donor concentration $N_D = 1.7 \cdot 10^{17}$ cm^{-3} and $N_D = 5.3 \cdot 10^{16}$ cm^{-3} is obtained for fresh and degraded capacitor respectively. Such decrease in donor concentration in the depletion layer at the cathode of degraded capacitors is a result of the accumulation of positively charged defects (ionized oxygen vacancies). Hence, the obtained values give a valuable insight into the mechanism underlying the process of aging in MLCCs. On the other hand, an accurate quantitative evaluation from KPFM data would need to take in account several factors, for which corrections should be estimated: i. The averaging effect of the tip cone and cantilever operating in KPFM mode [39–41]; ii. Presence of adsorbates, if not operating in a controlled environment; iii. Difference between bulk and surface work function due to surface band bending arising from presence of surface states [13,14,37]. For instance, it is well known that the presence of interface states [35,42] at the BTO-Ni interface is the reason for the discrepancy between barrier height values as by Schottky-Mott rule [35] (ϕ_B = 1.2eV) and experimentally measured (0.68eV [11] and 0.63eV [30]). Likewise, a surface technique (such as KPFM) detects the surface band structure, which is different form the bulk one due to surface states leading surface band bending [14].

Hence, while these matters do not affect extraction of qualitative information as in the present investigations, for quantitative information measurements in a controlled atmosphere [14,17] would be recommended. Additionally, sample preparation with a procedure apt to limit formation of surface states (such as cleavage might be, which however is not suitable for

MLCCs) on the exposed face of the sample would yield measurements of a configuration closer to the actual bulk band structure.

CONCLUSIONS

In summary, this work finally provides direct evidence of the nanoscale electrical phenomenon underlying insulation degradation in MLCCs, which has been elusive for over a decade. Evolution of potential barriers at the interfaces of degrading Ni-BTO MLCCs is investigated by KPFM. Discontinuities in potential gradient at the interfaces acquired by KPFM are shown to be related to the presence of potential barriers. A trend is revealed, in which, with degradation of the device, the barriers at the HALT cathode decrease, while barriers at the HALT anode are hardly affected.

These findings agree with the mechanism proposed for insulation resistance degradation over a decade ago, based on macroscopic electrical measurements and TEM investigations [9], where oxygen vacancies electromigration leads to a transition at the metal-dielectric interface from Schottky to Ohmic contact. The agreement is evidenced by relating the KPFM measurement in this work to the band diagrams in fresh and degraded capacitors expected for the proposed mechanism.

Further proof of the correspondence of the detected discontinuities in KPFM potential derivative with presence of potential barriers at the interfaces is provided by experiments performed with increasing external bias, showing disappearance of discontinuities at the electrode interface where band flattening is expected.

We show that KPFM offers the possibility for in depth studies of barriers at metal-dielectric interfaces in MLCCs, with further space for extraction of quantitative data, provided more controlled experimental conditions are achieved. As well, study of early-stage degradation by monitoring evolution of barriers at the metal-dielectric interface and at the grain boundaries will be possible in more stable environment and with progressively degraded samples.

AUTHOR INFORMATION

Corresponding author:

* E-mail address: a.morelli@ulster.ac.uk; alessio.morelli.pfm@gmail.com

ACKNOWLEDGEMENT

We wish to acknowledge funding from Invest Northern Ireland (RD0713920). A.M. acknowledges funding from the European Union's INTERREG VA Programme, managed by the Special EU Programmes Body (SEUPB).

ASSOCIATED CONTENT

Supporting Information: Band diagram inclusive of barriers at grain boundaries; Additional forward and reverse KPFM maps at 1V applied bias; Full set of KPFM maps with increasing bias.

REFERENCES

[1] Sakabe, Y., Multilayer ceramic capacitors, Curr. Opin. Solid State Mater. Sci. 2 (1997) 584–587. https://doi.org/10.1016/S1359-0286(97)80049-6.

[2] Kishi, H.; Mizuno, Y.; Chazono, H., Base-metal electrode-multilayer ceramic capacitors: Past, present and future perspectives, Japanese J. Appl. Physics, Part 1 Regul. Pap. Short Notes Rev. Pap. 42 (2003) 1–5. https://doi.org/10.1143/jjap.42.1.

[3] Hong, K.; Lee, T.H.; Suh, J.M.; Yoon, S.H.; Jang, H.W., Perspectives and challenges in multilayer ceramic capacitors for next generation electronics, J. Mater. Chem. C. 7 (2019) 9782–9802. https://doi.org/10.1039/c9tc02921d.

[4] Yamamatsu, J.; Kawano, N.; Arashi, T.; Sato, A.; Nakano, Y.; Nomura, T., Reliability of multilayer ceramic capacitors with nickel electrodes, J. Power Sources. 60 (1996) 199–203. https://doi.org/10.1016/S0378-7753(96)80011-5.

[5] Yang, G.Y.; Dickey, E.C.; Randall, C.A.; Barber, D.E.; Pinceloup, P.; Henderson, M.A.; Hill, R.A.; Beeson, J.J.; Skamser, D.J., Oxygen nonstoichlometry and dielectric evolution of BaTiO 3. Part I - Improvement of insulation resistance with reoxidation, J. Appl. Phys. 96 (2004) 7492–7499. https://doi.org/10.1063/1.1809267.

[6] Yang, G.Y.; Dickey, E.C.; Randall, C.A.; Randall, M.S.; Mann, L.A., Modulated and ordered defect structures in electrically degraded Ni-BaTiO3 multilayer ceramic capacitors, J. Appl. Phys. 94 (2003) 5990–5996. https://doi.org/10.1063/1.1615300.

[7] Genenko, Y.A.; Glaum, J.; Hoffmann, M.J.; Albe, K., Mechanisms of aging and fatigue in ferroelectrics, Mater. Sci. Eng. B Solid-State Mater. Adv. Technol. 192 (2015) 52–82. https://doi.org/10.1016/j.mseb.2014.10.003.

[8] Chazono, H.; Kishi, H., dc-electrical degradation of the BT-based material for multilayer ceramic capacitor with Ni internal electrode: Impedance analysis and microstructure, Japanese J. Appl. Physics, Part 1 Regul. Pap. Short Notes Rev. Pap. 40 (2001) 5624–5629. https://doi.org/10.1143/jjap.40.5624.

[9] Yang, G.Y.; Lian, G.D.; Dickey, E.C.; Randall, C.A.; Barber, D.E.; Pinceloup, P.; Henderson, M.A.; Hill, R.A.; Beeson, J.J.; Skamser, D.J., Oxygen nonstoichiometry and dielectric evolution of BaTiO 3. Part II- Insulation resistance degradation under applied dc bias, J. Appl. Phys. 96 (2004) 7500–7508. https://doi.org/10.1063/1.1809268.

[10] Izawa, K.; Sada, T.; Utsunomiya, M.; Inayama, S.; Fujikawa, N.; Matsubara, K.; Yasukawa, K., Direct observation of cross sectional local conductive paths in a degraded

multilayered ceramic capacitor, Appl. Phys. Lett. 116 (2020) 192903. https://doi.org/10.1063/5.0003962.

[11] Long, D.M.; Klein, A.; Dickey, E.C., Barrier formation at BaTiO 3 interfaces with Ni and NiO, Appl. Surf. Sci. 466 (2019) 472–476. https://doi.org/10.1016/j.apsusc.2018.10.040.

[12] Nonnenmacher, M.; O'Boyle, M.P.; Wickramasinghe, H.K., Kelvin probe force microscopy, Appl. Phys. Lett. 58 (1991) 2921–2923. https://doi.org/10.1063/1.105227.

[13] Shikler, R.; Meoded, T.; Fried, N.; Rosenwaks, Y., Potential imaging of operating light-emitting devices using Kelvin force microscopy, Appl. Phys. Lett. 74 (1999) 2972–2974. https://doi.org/10.1063/1.123983.

[14] Saraf, S.; Rosenwaks, Y., Local measurement of semiconductor band bending and surface charge using Kelvin probe force microscopy, Surf. Sci. 574 (2005). https://doi.org/10.1016/j.susc.2004.10.042.

[15] Kikukawa, A.; Hosaka, S.; Imura, R., Silicon pn junction imaging and characterizations using sensitivity enhanced Kelvin probe force microscopy, Appl. Phys. Lett. 66 (1995) 3510–3512. https://doi.org/10.1063/1.113780.

[16] Brooks, W.S.M.; Irvine, S.J.C.; Taylor, D.M., Scanning Kelvin probe measurements on As-doped CdTe solar cells, Semicond. Sci. Technol. 28 (2013). https://doi.org/10.1088/0268-1242/28/10/105024.

[17] Suzuki, K.; Okamoto, T.; Kondo, H.; Tanaka, N.; Ando, A., Insulation degradation behavior of multilayer ceramic capacitors clarified by Kelvin probe force microscopy under ultra-high vacuum, J. Appl. Phys. 113 (2013). https://doi.org/10.1063/1.4791714.

[18] Okamoto, T.; Kitagawa, S.; Inoue, N.; Ando, A., Electric field concentration in the vicinity of the interface between anode and degraded BaTiO3 -based ceramics in multilayer ceramic capacitor, Appl. Phys. Lett. 98 (2011). https://doi.org/10.1063/1.3555466.

[19] Hong, K.; Lee, T.H.; Suh, J.M.; Park, J.S.; Kwon, H.S.; Choi, J.; Jang, H.W., Direct Observation of Surface Potential Distribution in Insulation Resistance Degraded Acceptor-Doped BaTiO3 Multilayered Ceramic Capacitors, Electron. Mater. Lett. 14 (2018) 629–635. https://doi.org/10.1007/s13391-018-0066-6.

[20] Heywang, W., Semiconducting barium titanate, J. Mater. Sci. 6 (1971) 1214–1224. https://doi.org/10.1007/BF00550094.

[21] Smyth, D.M., Defect structure in perovskite titanates, Curr. Opin. Solid State Mater. Sci. 1 (1996) 692–697. https://doi.org/10.1016/S1359-0286(96)80053-2.

[22] Masó, N.; Prades, M.; Beltrán, H.; Cordoncillo, E.; Sinclair, D.C.; West, A.R., Field enhanced bulk conductivity of acceptor-doped BaTi1−xCaxO3−x ceramics, Appl. Phys. Lett. 97 (2010) 062907. https://doi.org/https://doi.org/10.1063/1.3476355.

[23] Huang, C.M.; Lin, C.Y.; Shieh, J., Relationship between the evolutions of the microstructure and semiconductor properties of yttrium-doped barium titanate ceramics, J. Phys. D. Appl. Phys. 44 (2011). https://doi.org/10.1088/0022-3727/44/34/345403.

[24] Minford, W.J., Accelerated Life Testing and Reliability of High K Multilayer Ceramic Capacitors, IEEE Trans. Components, Hybrids, Manuf. Technol. 5 (1982) 297–300. https://doi.org/10.1109/TCHMT.1982.1135974.

[25] Randall, C.A.; Maier, R.; Qu, W.; Kobayashi, K.; Morita, K.; Mizuno, Y.; Inoue, N.; Oguni, T., Improved reliability predictions in high permittivity dielectric oxide capacitors under high dc electric fields with oxygen vacancy induced electromigration, J. Appl. Phys. 113 (2013). https://doi.org/10.1063/1.4772599.

[26] Horcas, I.; Fernández, R.; Gómez-Rodríguez, J.M.; Colchero, J.; Gómez-Herrero, J.;

Baro, A.M., WSXM: A software for scanning probe microscopy and a tool for nanotechnology, Rev. Sci. Instrum. 78 (2007). https://doi.org/10.1063/1.2432410.

[27] Tsur, Y.; Randall, C.A., How trivalent amphoteric dopants in BaTiO3 ceramics improve reliability of capacitors, AIP Conf. Proc. 535 (2000) 283–287. https://doi.org/10.1063/1.1324465.

[28] Li, Y.; Hao, Y.; Wang, X.; Yao, X., Studies of Dielectric Properties of Rare Earth (Y, Gd, Yb) Doped Barium Titanate Sintered in Pure Nitrogen, Ferroelectrics. 407 (2010) 134–139. https://doi.org/10.1080/00150193.2010.484757.

[29] Polotai, A. V.; Jeong, T.H.; Yang, G.Y.; Dickey, E.C.; Randall, C.A.; Pinceloup, P.; Gurav, A.S., Effect of Cr additions on the electrical properties of Ni-BaTiO3 ultra-thin multilayer capacitors, J. Electroceramics. 23 (2009) 6–12. https://doi.org/10.1007/s10832-008-9496-0.

[30] Levi, R.D.; Samantaray, M.M.; Trolier-Mckinstry, S.; Randall, C.A., Influence of substrate microstructure on the high field dielectric properties of BaTiO3 films, J. Appl. Phys. 104 (2008). https://doi.org/10.1063/1.3013448.

[31] Cann, D.P.; Maria, J.P.; Randall, C.A., Relationship between wetting and electrical

contact properties of pure metals and alloys on semiconducting barium titanate ceramics, J. Mater. Sci. 36 (2001) 4969–4976. https://doi.org/10.1023/A:1011817128242.

[32] Eastman, D.E., Photoelectric Work Functions of Transition, Rare-Earth, and Noble Metals, Phys. Rev. B. 2 (1970) 1–2. https://doi.org/10.1103/PhysRevB.2.1.

[33] Yoo, H.I.; Chang, M.W.; Oh, T.S.; Lee, C.E.; Becker, K.D., Electrocoloration and oxygen vacancy mobility of BaTi O3, J. Appl. Phys. 102 (2007). https://doi.org/10.1063/1.2802290.

[34] Marri, I.; Ossicini, S., Oxygen vacancy effects on the Schottky barrier height at the Au/TiO2(110) interface: A first principle study, Solid State Commun. 147 (2008) 205–207. https://doi.org/10.1016/j.ssc.2008.05.018.

[35] Tung, R.T., The physics and chemistry of the Schottky barrier height, Appl. Phys. Rev. 1 (2014). https://doi.org/10.1063/1.4858400.

[36] Dietz, G.W.; Schumacher, M.; Waser, R.; Streiffer, S.K.; Basceri, C.; Kingon, A.I., Leakage currents in Ba0.7Sr0.3TiO3 thin films for ultrahigh-density dynamic random access memories, J. Appl. Phys. 82 (1997) 2359–2364. https://doi.org/10.1063/1.366045.

[37] Sze, S.M.; Ng, K.K., Physics of semiconductor devices, 3rd ed., John Wiley & Sons, 2007.

[38] Liu, D.D., Insulation resistance degradation in Ni-BaTiO3 multilayer ceramic capacitors, IEEE Trans. Components, Packag. Manuf. Technol. 5 (2015) 40–48. https://doi.org/10.1109/TCPMT.2014.2374576.

[39] Hochwitz, T., Capacitive effects on quantitative dopant profiling with scanned electrostatic force microscopes, J. Vac. Sci. Technol. B Microelectron. Nanom. Struct. 14 (1996) 457. https://doi.org/10.1116/1.588494.

[40] Vatel, O.; Tanimoto, M., Kelvin probe force microscopy for potential distribution measurement of semiconductor devices, J. Appl. Phys. 77 (1995) 2358–2362. https://doi.org/10.1063/1.358758.

[41] Charrier, D.S.H.; Kemerink, M.; Smalbrugge, B.E.; de Vries, T.; Janssen, R.A.J., Real versus measured surface potentials in scanning Kelvin probe microscopy, ACS Nano. 2 (2008) 622–626. https://doi.org/10.1021/nn700190t.

[42] Mönch, W., Metal-semiconductor contacts: electronic properties, Surf. Sci. 299–300 (1994) 928–944. https://doi.org/https://doi.org/10.1016/0039-6028(94)90707-2.

FOR TABLE OF CONTENTS ONLY